Journal of Computational Physics 445 (2021) 110626

Contents lists available at ScienceDirect

Journal of Computational Physics

www.elsevier.com/locate/jcp

Contour dynamics for one-dimensional Vlasov-Poisson plasma with the periodic boundary

Hiroki Sato, T.-H. Watanabe *, S. Maeyama

Department of Physics, Nagoya University, Furo-cho, Nagoya, 4646-8602, Japan

ARTICLE INFO

Article history:
Available online 11 August 2021

Keywords:
Contour dynamics
Vlasov equation
Landau damping

ABSTRACT

We revisit the contour dynamics (CD) simulation method which is applicable to large deformation of distribution function in the Vlasov-Poisson plasma with the periodic boundary, where contours of distribution function are traced without using spatial grids. Novelty of this study lies in application of CD to the one-dimensional Vlasov-Poisson plasma with the periodic boundary condition. A major difficulty in application of the periodic boundary is how to deal with contours when they cross the boundaries. It has been overcome by virtue of a periodic Green's function, which effectively introduces the periodic boundary condition without cutting nor reallocating the contours. The simulation results are confirmed by comparing with an analytical solution for the piece-wise constant distribution function in the linear regime and a linear analysis of the Landau damping. Also, particle trapping by Langmuir wave is successfully reproduced in the nonlinear regime.

1. Introduction

Kinetic equations for plasma dynamics describe many interesting physical phenomena, but are generally difficult to be solved analytically or numerically. For example, a long term nonlinear evolution of the distribution function is not yet fully understood even in the one-dimensional Vlasov-Poisson system. Three types of simulation methods for kinetic plasma are widely known, such as Lagrangian, semi-Lagrangian, and Eulerian methods. The Particle-In-Cell (Lagrangian) method has a problem of numerical noise, while resolution of the Vlasov method (Eulerian) is limited by the grid size. Indeed, it is shown that, in the Vlasov simulation of the nonlinear Landau damping, fine structures of the distribution function continue to grow in phase space and are stretched exponentially in time, increasing numerical errors (Ref. [1]).

The water-bag model, which assumes a piece-wise constant distribution function (f), has been studied for the Vlasov-Poisson plasma (Refs. [2–4]) since 1960s, and successfully resolved stretching and strong deformation of f in the phase space (x, v). In 1979, as a generalization of the water-bag model, contour dynamics (CD) method is introduced by Zabusky, Hughes, and Roberts (Ref. [5]) for solving inviscid and incompressible fluid motions in the two-dimensional configuration space (x, y). The CD method employs nodes on each contour of which motion is given by calculating line integrals of the Green's function along contours. Because CD employs no spatial grid but nodes on contours (Lagrangian), the numerical resolution is not limited by spatial grids, which makes the CD method tough against large deformation of vorticity (Ref. [6]).

In this paper, we revisit the CD method and apply it to the Vlasov-Poisson plasma with the periodic boundary condition. Although the basic idea of the CD method stems from the water-bag model, there has been a few applications to the

* Corresponding author.
E-mail address: watanabe.tomohiko@nagoya-u.jp (T.-H. Watanabe).

https://doi.org/10.1016/j.jcp.2021.110626
0021-9991/

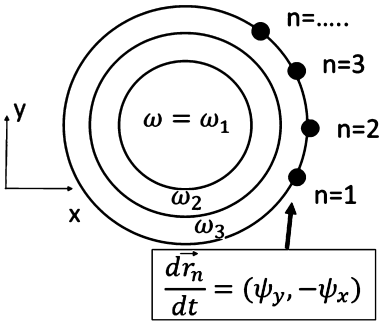

Fig. 1. In contour dynamics, motion of the contours are determined by solving the Hamilton equations of the node points.

Vlasov-Poisson plasma. The CD method differs from the water-bag model as no spatial grid is used in the former in solving Poisson equation (Ref. [2]). Although a modern implementation of the water-bag method by Colombi & Touma (Ref. [7]) did not use spatial grids, the application is limited to a system with no spatial boundary. Novelty of the present paper lies in application of the CD method to the Vlasov-Poisson plasma with the periodic boundary, where we consider time development of contours of the distribution function without using spatial grids. The simulation results are confirmed by comparing with an analytical solution for the piece-wise constant distribution function in the linear regime and a linear analysis of the Landau damping. Furthermore, the particle trapping by Langmuir waves is successfully reproduced in the nonlinear regime. Here, it should be remarked that no contour surgery (Ref. [8]) nor node redistributions (Ref. [9]) is employed in numerical simulations in this paper, because we focus on validity of our implementation for the periodic boundary condition.

This article is organized as follows. After a brief introduction to the CD in Section 2, application to the Vlasov-Poisson system with the periodic boundary is described in Section 3. Validity of the CD method is confirmed by comparing the simulation results with the analytical solution for the piece-wise constant distribution function in Section 4. A bench mark test for the linear Landau damping is described in Section 5.1. Application to the nonlinear Landau damping is shown in Section 5.2. Finally, we summarize the results in Section 6.

2. Contour dynamics

Zabusky, Hughes, and Roberts have proposed contour dynamics algorithm for the Euler equation of fluid dynamics in two dimensions (Ref. [5]). The governing equations are

$$\frac{D\omega}{Dt} = \frac{\partial\omega}{\partial t} + u\frac{\partial\omega}{\partial x} + v\frac{\partial\omega}{\partial y} = 0, \tag{1}$$

$$\nabla^2\psi = \frac{\partial^2\psi}{\partial x^2} + \frac{\partial^2\psi}{\partial y^2} = -\omega, \tag{2}$$

$$u = \frac{\partial\psi}{\partial y}, v = -\frac{\partial\psi}{\partial x},$$

$$\omega = -\frac{\partial u}{\partial y} + \frac{\partial v}{\partial x}, \tag{3}$$

where ψ is the stream function and ω means the vorticity. Time development of the vorticity is calculated by tracing motions of contours of the piece-wise constant vorticity distribution. The flow velocity is given by the line integrals of the Green's function on the contours, such that

$$(u, v) = \left(\frac{\partial\psi}{\partial y}, -\frac{\partial\psi}{\partial x}\right) = \sum_m (\Delta\omega_m) \oint_{C_m} G(x, y; \xi, \eta) dr'_m, \tag{4}$$

where m is a label of contours, C_m is the contour labeled by m, and $\Delta\omega_m$ is a jump of vorticity when crossing the contour C_m inward. The two-dimensional Green's function, $G(x, y; \xi, \eta)$, is given as

$$G(x, y; \xi, \eta) = -\frac{1}{2\pi}\log\sqrt{(x-\xi)^2 + (y-\eta)^2}. \tag{5}$$

The contours are discretized by nodes with label n, and motion of the contours is determined by solving the Hamilton equations of the node points (Fig. 1). Each contour represents a constant vorticity line, and is advected by an incompressible flow as given in Eq. (1). The incompressibility also guarantees conservation of volumes surrounded by each contour.

3. Application to Vlasov-Poisson system

3.1. Basic scheme

Here, we consider application of the CD method to the Vlasov-Poisson system with the periodic boundary. The normalized Vlasov-Poisson equations are

$$\frac{\partial f}{\partial \tau} + v\frac{\partial f}{\partial x} + a\frac{\partial f}{\partial v} = 0, \tag{6}$$

$$a = \frac{\partial \phi}{\partial x}, \tag{7}$$

$$-\nabla^2\phi = 1 - \int_{-\infty}^{\infty} f(x,v)dv =: F(x), \tag{8}$$

where f is the distribution function of electrons, while stationary background ions are assumed. The particle density is normalized so that $\int_{-L/2}^{L/2} dx \int_{-\infty}^{\infty} dv f(x.v) = L$, where L denotes the system length. The periodic boundary conditions at $x = \pm L/2$ are given by

$$\lim_{\epsilon\to -0}\phi\left(\frac{L}{2}+\epsilon\right) = \lim_{\epsilon'\to +0}\phi\left(-\frac{L}{2}+\epsilon'\right), \tag{9}$$

$$\lim_{\epsilon\to -0}\phi'\left(\frac{L}{2}+\epsilon\right) = \lim_{\epsilon'\to +0}\phi'\left(-\frac{L}{2}+\epsilon'\right) \text{ (quasi neutrality)}. \tag{10}$$

The Liouville's theorem and Eq. (6) guarantee the volume conservation and $\frac{df}{d\tau} = 0$, which are required for contour dynamics method. In order to implement the CD, we employ the Green's function, G, that satisfies

$$\nabla^2 G(x;\xi) = \frac{1}{L} - \delta(x-\xi), \tag{11}$$

$$\lim_{\epsilon\to -0} G\left(\frac{L}{2}+\epsilon\right) = \lim_{\epsilon'\to +0} G\left(-\frac{L}{2}+\epsilon'\right), \tag{12}$$

$$\lim_{\epsilon\to -0} G'\left(\frac{L}{2}+\epsilon\right) = \lim_{\epsilon'\to +0} G'\left(-\frac{L}{2}+\epsilon'\right). \tag{13}$$

Solving Eqs. (11), (12), and (13) to obtain G (Ref. [10]), one finds

$$G(x;\xi) = \frac{1}{2L}\left(|x-\xi| - \frac{L}{2}\right)^2. \tag{14}$$

Therefore,

$$\phi(x) = \int_{-\frac{L}{2}}^{\frac{L}{2}} G(x;\xi)\,F(\xi)\,d\xi + \text{const} \quad \text{for } x \in \left(-\frac{L}{2}, \frac{L}{2}\right). \tag{15}$$

The acceleration of each particle at x is given by the CD representation,

$$a(x) = \sum_m^{N_m} \Delta f_m \oint_{C_m} G(x;\xi)\,dv, \tag{16}$$

where N_m is the number of contours, C_m is a contour labeled by m and Δf_m is the jump of distribution function when crossing the contour C_m inward. We discretize the contours with nodes labeled counterclockwise by n and connect nodes with straight line segments. Then, Eq. (16) breaks down into

$$a(x) = \sum_m^{N_m} \Delta f_m \sum_n \frac{v_{n+1}-v_n}{2}\left(\frac{w_n^2(x)}{L} + \frac{\delta_n^2}{12L} - I_n(x)\right), \tag{17}$$

where

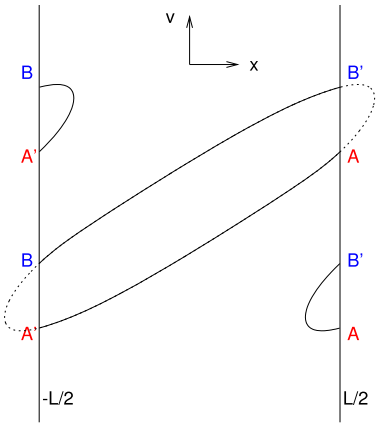

Fig. 2. Conventional implementation of the periodic boundary. Contours which get out of simulation box are cut and reallocated (A, B, A' and B' are defined on Eqs. (21) and (22)).

$$I_n(x) = \begin{cases} |w_n(x)| & \text{for } |w_n(x)| \geq \frac{\delta_n}{2} \\ \frac{w_n^2(x)}{\delta_n} + \frac{\delta_n}{4} & \text{for } |w_n(x)| < \frac{\delta_n}{2} \end{cases} \text{ with } w_n(x) := x - \frac{x_{n+1}+x_n}{2} \text{ and } \delta_n := |x_{n+1} - x_n|. \tag{18}$$

Although n is a function of the label of contours (m), we use the notation of $n = n(m)$ for simplicity. Equation of motion of each node point labeled by i is given by

$$\frac{d^2 x_i}{d\tau^2} = a\,(x = x_i) = \sum_m^{N_m} \Delta f_m \sum_n \frac{v_{n+1} - v_n}{2} \left(\frac{w_n^2(x_i)}{L} + \frac{\delta_n^2}{12L} - I_n(x_i) \right). \tag{19}$$

For the time integration, we use the leap-frog scheme with the time step size $\Delta\tau = 0.01$ in the all simulations shown below.

3.2. Implementation of the periodic boundary

A difficulty of implementation arises in the CD method with the periodic boundary, when a node (x_n, v_n) moves across the boundaries and comes into the simulation box from the another side. Straightforwardly, we may cut the contour at the boundary and reallocate a node point (x_n, v_n) as

$$x_n \notin (-L/2, L/2) \Rightarrow \begin{cases} x_n \mapsto x_n - L/2 & ;\text{if } L/2 < x_n \\ x_n \mapsto x_n + L/2 & ;\text{if } x_n < -L/2 \end{cases} \tag{20}$$

and make interpolation of points $(\tilde{x_s}, \tilde{v_s})$ and $(\tilde{x_t}, \tilde{v_t})$ on the boundary between $(x_{n+1}, v_{n+1}) \notin \left(\frac{-L}{2}, \frac{L}{2}\right)$ and $(x_n, v_n) \in \left(\frac{-L}{2}, \frac{L}{2}\right)$,

$$(\tilde{x_s}, \tilde{v_s}) = \begin{cases} \left(\frac{L}{2}, \frac{v_{n+1}-v_n}{x_{n+1}-x_n} \left(\frac{L}{2} - x_{n+1} \right) + v_{n+1} \right) & ;\text{if } L/2 \leq x_{n+1} \quad \cdots A \\ \left(\frac{-L}{2}, \frac{v_{n+1}-v_n}{x_{n+1}-x_n} \left(\frac{-L}{2} - x_{n+1} \right) + v_{n+1} \right) & ;\text{if } x_{n+1} \leq -L/2 \quad \cdots B \end{cases} \tag{21}$$

$$(\tilde{x_t}, \tilde{v_t}) = \begin{cases} \left(\frac{-L}{2}, \frac{v_{n+1}-v_n}{x_{n+1}-x_n} \left(\frac{L}{2} - x_{n+1} \right) + v_{n+1} \right) & ;\text{if } L/2 \leq x_{n+1} \quad \cdots A' \\ \left(\frac{L}{2}, \frac{v_{n+1}-v_n}{x_{n+1}-x_n} \left(\frac{-L}{2} - x_{n+1} \right) + v_{n+1} \right) & ;\text{if } x_{n+1} \leq -L/2 \quad \cdots B' \end{cases} \tag{22}$$

for calculation of the line integrals (See Fig. 2). Here, we call this method the reallocation scheme. Since we must know the sequence of the nodes for the CD method, the reallocated nodes complicate the computational algorithm. Actually, we need to count how many times each node moved across the boundaries and to use the counts every time in calculation of $\frac{v_{n+1}-v_n}{2} \left(\frac{w_n^2}{L} + \frac{\delta_n^2}{12L} - I_n \right)$. However, it increases numerical costs and makes the code implementation complicated.

In the following, we propose a novel scheme to implement the periodic boundary in CD, which is named a periodic Green's function method. Because we consider the periodic problem; $f(a) = f(a+L)$, $\phi(a) = \phi(a+L)$, and $\phi'(a) = \phi'(a+L)$. Thus, it may be possible to eliminate the boundaries at $x = \pm\frac{L}{2}$, while extending the simulation box to $(-\infty, \infty)$ and imposing the periodicity to the Green's function, that is,

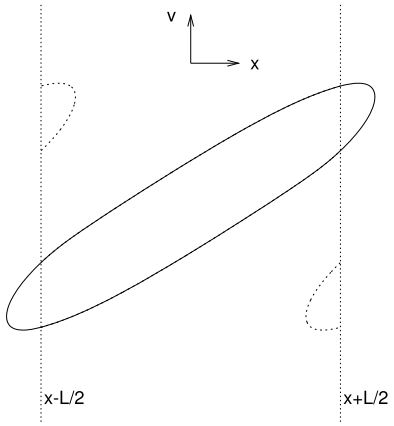

Fig. 3. Implementation of the periodic boundary using $G' = G(Mod(\xi - (x - L/2), L) + (x - L/2); x)$. The periodic boundary is effectively introduced without cutting nor reallocating the contours.

$$\forall x \in (-\infty, \infty), \quad a(x) = \sum_{m=1}^{N_m} \Delta f_m \oint_{c_m} G'(x;\xi)\, dv', \tag{23}$$

with

$$G'(x;\xi) = G(x; Mod(\xi - (x - L/2), L) + (x - L/2)), \tag{24}$$

where

$$Mod(a,b) = Min\{c\,(\geq 0)\,|\exists r \in \mathbb{Z}, a = br + c\}. \tag{25}$$

In this way, we can avoid cutting or reallocation of the contours, but equivalently the contours feel the periodicity of the system through G' instead of G (See Fig. 3). If $\forall n, |x_n - x_{n-1}| < \frac{L}{2}$ is satisfied, then (17) becomes

$$a(x) = \sum_{m}^{N_m} \Delta f_m \sum_{n} \frac{v_{n+1} - v_n}{2} \left(\frac{w_n'^2}{L} + \frac{\delta_n^2}{12L} - I_n' \right), \tag{26}$$

where

$$w_n'(x) := x + r(x_n, x)\, L - \frac{x_{n+1} + x_n}{2}, \tag{27}$$
$$r(x_n, x) := \frac{x_n - \left(x - \frac{L}{2}\right) - Mod\left(x_n - \left(x - \frac{L}{2}\right), L\right)}{L} = \lfloor \frac{x_n - \left(x - \frac{L}{2}\right)}{L} \rfloor,$$

and

$$\delta_n := |x_{n+1} - x_n|, \quad I_n'(x) = \begin{cases} |w_n'(x)| & \text{for } |w_n'(x)| \geq \frac{\delta_n}{2} \\ \frac{w_n'^2(x)}{\delta_n} + \frac{\delta_n}{4} & \text{for } |w_n'(x)| < \frac{\delta}{2} \end{cases}. \tag{28}$$

Here, the periodicity is introduced not in C_m, but in G'. Therefore we do not need to count how many times each node moves across the boundaries, which makes a faster and simpler implementation. Our new implementation with the periodic Green's function G' accelerate the computation speed about 1.5 faster than that of the reallocation scheme. It owes to no cutting nor reallocation, which makes the code avoid many "if" branches.

4. Benchmark test for piece-wise constant distribution function

In order to check validity of our application, we consider the initial distribution function given by

$$f(x, v, \tau = 0) = \sum_{m=-N_m}^{N_m} b_m U(v - v_m(x, 0)), \tag{29}$$

$$U(x) = \begin{cases} 1 & 0 < x \\ 0 & x \leq 0 \end{cases}, \tag{30}$$

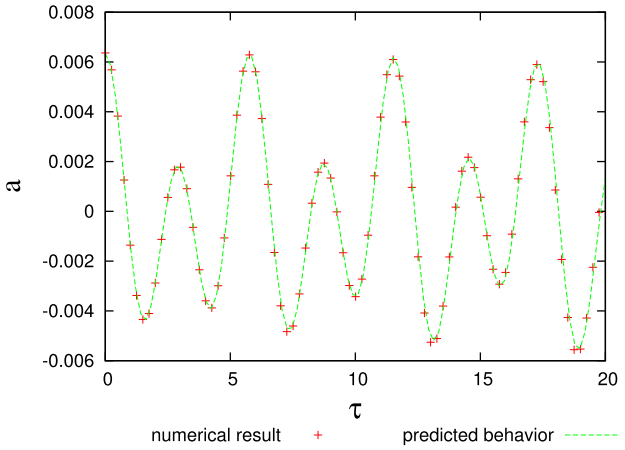

Fig. 4. Benchmark test1: Time evolution of $a = \partial\phi/\partial x$. Red points are simulation results and green line is predicted by Eq. (32). $N_m = 2$, $b_1 = b_2 = -1/6$, $\Delta v = 1.0$, $k = 1.0$ and $\alpha = 0.01$ are given for initial distribution function in Eq. (29).

where $b_m = -b_{-m} < 0$ and $v_m(x,0) = v_m^0 + v_m^1(x)$. Also $v_m^0 = m\Delta v$ and $v_m^1(x) = \alpha e^{ikx}$ with $\Delta v \in \mathbb{R}^+$ and $kL/2\pi \in \mathbb{N}$, where $\alpha \ll 1$ so that $|v_m^1| \ll |v_m^0|$. This function Eq. (29) was also used to study the water-bag model (Ref. [11]). As shown in Appendix, the linear dispersion relation is derived as

$$D(\omega) = 1 + \sum_{m>0} \frac{2b_m v_m^0}{\omega^2 - \left(kv_m^0\right)^2} = 0. \tag{31}$$

Solving the initial value problem analytically, the acceleration $a(x,\tau)$ is determined by means of ω_l which satisfies $D(\omega_l) = 0$ with $kv_l^0 < \omega_l < kv_{l+1}^0$,

$$a(x,\tau) = Re\left[\sum_{j>0} \frac{\sum_{m>0}\left\{(-b_m)\,\alpha e^{i(kx-\frac{\pi}{2})}\Pi_{n(\neq m)>0}\left(\left(\omega_j\right)^2 - \left(kv_n^0\right)^2\right)\right\}}{k\Pi_{n(\neq j)>0}\left(\omega_j^2 - \omega_n^2\right)} 2\cos\omega_j\tau\right]. \tag{32}$$

We make comparison of a simulation result with Eqs. (31) and (32).

For $N_m = 2$, $b_1 = b_2 = -1/6$, $\Delta v = 1.0$, $k = 1.0$ and $\alpha = 0.01$, Eqs. (31) and (32) lead $a(x = -1.4\pi, \tau) = A_1\cos(\omega_1\tau) + A_2\cos(\omega_2\tau)$ with $A_1 = 0.00226$, $A_2 = 0.00409$, $\omega_1 = 1.13$ and $\omega_2 = 2.18$. The numerical result of $a(x = -1.4\pi, \tau)$ shown in Fig. 4 agrees well with the analytical prediction, Eq. (32). It shows validity of our implementation of the CD method for the Vlasov-Poisson system with the periodic boundary condition.

5. Benchmark test for the Landau damping

5.1. Linear Landau damping

We also verify our code for the linear Landau damping. We set the initial contour distribution as follows. The initial (continuous) distribution function f is given by

$$f(x,v,\tau=0) = \frac{1}{\sqrt{2\pi}}\exp\left(-\frac{v^2}{2}\right)(1+\alpha\cos(kx)). \tag{33}$$

By means of a sequence $\{\Delta f_m\}_{m=1}^{N_{Max}} : \Delta f_m \in \mathbb{R}^+$ and $\sum_{m=1}^{N_{Max}} \Delta f_m < \underset{x,v\in\mathbb{R}}{Max}\{f(x,v,\tau=0)\}$, we define $\tilde{f}$, a piece-wise constant approximation of f,

$$\tilde{f}(x,v,\tau=0) := \sum_{m=1}^{N_{Max}} \Delta f_m I\left[\Sigma_{m'=1}^{m}\Delta f_{m'} < f(x,v,\tau=0)\right], \tag{34}$$

where

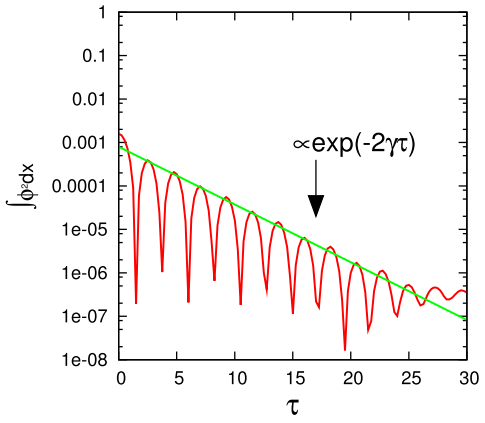

Fig. 5. Time history of the quadratic integral of the electrostatic potential ϕ obtained from the simulation of the linear Landau damping. The damping rate γ = -0.153 is successfully confirmed by the contour dynamics method.

$$I[P(x,v,\tau)] = \begin{cases} 1 & \text{if } P(x,v,\tau) \text{ is true} \\ 0 & \text{otherwise} \end{cases} \tag{35}$$

with a propositional function $P(x,v,\tau)$. However, Eq. (34) does not satisfy $\int_{-\frac{L}{2}}^{\frac{L}{2}} dx \int_{-\infty}^{\infty} \tilde{f}(x,v,t=0)dv = L$ because $\tilde{f}$ is a piece-wise constant function defined by means of contours of f. Therefore instead of $\tilde{f}$, we use $\tilde{f}'$ normalized by $(1+\epsilon)$,

$$\tilde{f}' = (1+\epsilon)\tilde{f}, \quad \text{where } \epsilon = \frac{L}{\int_{-\frac{L}{2}}^{\frac{L}{2}} dx \int_{-\infty}^{\infty} \tilde{f}(x,v,t=0)dv} - 1, \tag{36}$$

and thus $\Delta f'_m = (1+\epsilon)\Delta f_m$.

The simplest way of giving $\{\Delta f_m\}$ is $\Delta f_m =$ constant. However, contour dynamics method does not require constant Δf_m, and non-uniform contour intervals have an advantage over the constant Δf_m in approximation of f. In case with $\Delta f_m =$ constant, the contours are densely distributed where the velocity space gradient of f is steep around $v \sim \pm v_{th}$ (v_{th} means the thermal velocity), while no contour is found for $|v| > 3v_{th}$ when we use 40 contours. It means that there is no particle in $|v| > 3v_{th}$, while the super thermal particles can be included in the case of $\Delta f_m \neq$ constant. From the linear theory, real and imaginary parts of the eigenfrequency for $k = 0.5$ are evaluated as $\omega_r = 1.4156$ and $\gamma = -0.1533$. Thus, the phase velocity is $\omega_r/k \sim 2.8v_{th}$. This is the reason why the high speed particle should be included in this application. Otherwise, many contours are necessary in the constant Δf_m case in order to introduce contributions of the super thermal particles. Thus, we employ the non-uniform contour intervals of Δf_m which is defined as

$$\Delta f_m := \begin{cases} f(x = x_0, v = V_m) & m = 1 \\ f(x = x_0, v = V_m) - f(x = x_0, v = V_{m-1}) & 2 \le m \le N_{Max} \end{cases}, \tag{37}$$

with $dv \in \mathbb{R}^+, N_{Max} \in \mathbb{N}$ and $V_m := (N_{Max} + 1 - m)dv$. Since Eq. (33) has the maximum at $x = 0$, we set $x_0 = 0$. In this application, we used 40 contours with $dv = 0.1$, where the contour spacing in v is nearly constant covering the velocity space of $|v| < 4v_{th}$.

A simulation result for the linear Landau damping is presented in Fig. 5, where the initial distribution function is given by Eq. (37) with $\alpha = 0.01$ and $k = 0.5$. The simulation box size is $L = 4\pi$. We also used 2000 nodes/contour. One clearly finds the linear damping rate of $\gamma = -0.153$ successfully reproduced by the present CD method.

5.2. Nonlinear Landau damping

Next, we consider a benchmark test for the nonlinear Landau damping (Ref. [1]) with the initial distribution function in Eq. (33) where $\alpha = 0.5$ and $k = 0.5$. We employ 40 contours (with $N_{Max} = 40$ and $dv = 0.1$) and 8000 nodes/contour. It is noteworthy that intersections of contour lines are not observed till $\tau = 30$ in the present simulation. It is, thus, appropriate not to use the node redistribution nor the contour surgery in the current test case. Fig. 6 shows a snapshot of contour distribution in the phase space at $\tau = 30$, where the particle trapping by the Langmuir wave is successfully reproduced by the CD method.

Soundness of our implementation is also confirmed by conservation of energy, as shown in Fig. 7. Total energy, $E_t = \frac{1}{2}\iint v^2 f dx dv + \frac{1}{2}\int |\frac{\partial \phi}{\partial x}|^2 dx$, is conserved with an error, $\epsilon_{E(\tau)} = |E_t(\tau) - E_t(0)|/E(0)$, less than 2.5×10^{-5} for $\tau \le 30$.

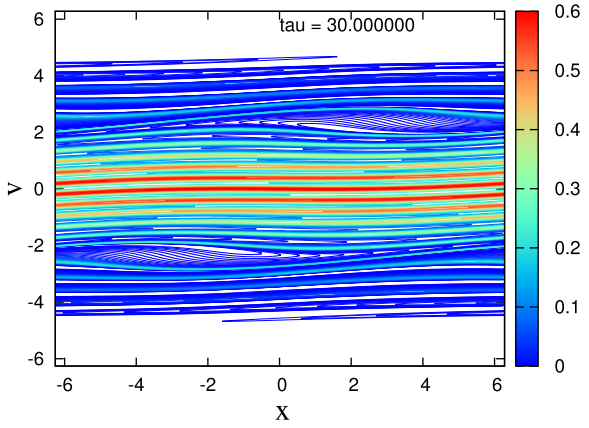

Fig. 6. Phase space structure of nonlinear Landau damping at $\tau = 30$. Particles trapped by waves are reproduced. The color bar represent the magnitude of f. (For interpretation of the colors in the figure(s), the reader is referred to the web version of this article.)

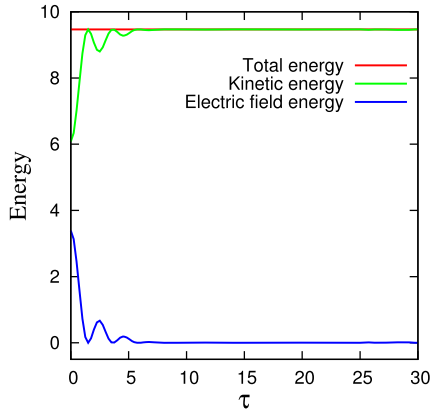

Fig. 7. Conservation of energy. Blue line represents energy of electric field, $E_\phi = \frac{1}{2}\int |\frac{\partial \phi}{\partial x}|^2 dx$, Green kinetic energy, $E_k = \frac{1}{2}\int\int v^2 f dx dv$, and Red Total energy, $E_t = E_\phi + E_k$.

Dependence of the numerical accuracy on the number of nodes per contour and the number of contours is investigated for conservation of the total energy and particles. Errors in the total energy conservation are shown in Figs. 8 (a) and (b) for cases with different numbers of nodes and contours, respectively. If the number of nodes per contour is decreased by 1/4 while using 40 contours, the total energy conservation significantly degrades after $\tau = 17$, which would be attributed to the contour crossing. Total energy conservation for different numbers of contour lines (but with 8000 nodes per contour) is also presented in Fig. 8 (b), where the maximum of numerical error in the case with 10 contours (with $N_{Max} = 10$ and $dv = 0.4$) is lower than that for the case of 2000 nodes/contour with 40 contours shown in Fig. 8 (a). Thus, the energy conservation is more sensitive to the number of nodes per contour than the number of contours.

Fig. 9 shows numerical errors found in the particle (or area) conservation, $\epsilon_N := |N(\tau) - N(0)|/N(0)$, for cases with different numbers of nodes and contours, where $N(\tau)$ is a total integral of the particle density defined as

$$N(\tau) := \iint \tilde{f}'(x, v, \tau) dx dv, \tag{38}$$

where

$$\tilde{f}'(x, v, \tau) := \sum_{m=1}^{N_{Max}} \Delta f'_m I[(x, v) \in S_m(\tau)] \tag{39}$$

with $S_m(\tau)$ denoting the closed polygonal region determined by nodes on the mth contour. Errors in the particle conservation, ϵ_N, is less than 10^{-4} for the case with 40 contours with 8000 nodes per contour (blue curve) while increasing in time. Generally speaking, the CD method tends to fail in following the strong deformation of contours with large curvature, because the contours consist of finite straight segments connected by nodes. This is confirmed in comparison for the different number of nodes shown in Fig. 9 (a), where the larger errors are found for the smaller number of nodes per contour. In comparison of Figs. 8 (b) and 9 (b), errors found in the energy and particle conservation for the case of 10 contours are correlated to each other, and are simultaneously improved by increasing the number of contours.

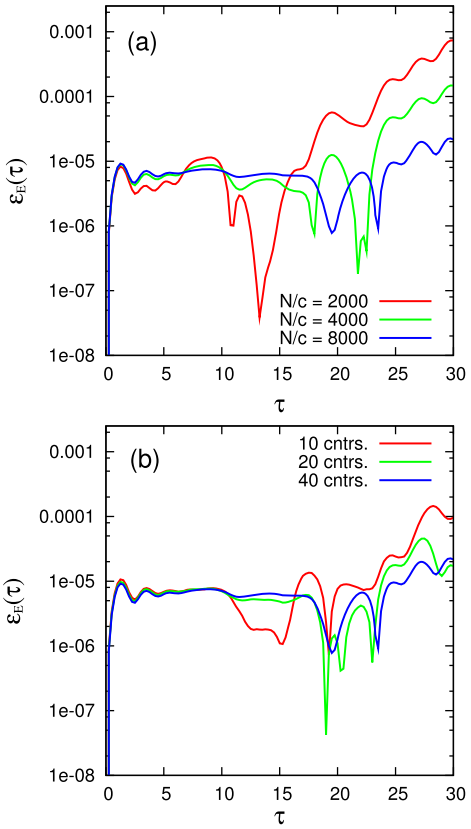

Fig. 8. Errors found in the total energy conservation, $\epsilon_E(\tau) = |E_t(\tau) - E_t(0)|/E(0)$, for cases with different numbers of (a) nodes per a contour (that is, 2000, 4000, and 8000 with 40 contours) or (b) contours (that is, $N_{Max} = 10$, 20, and 40 with 8000 nodes per contour but $dv = 0.4$, 0.2, and 0.1, respectively). Blue curves in (a) and (b) represent the same result in the case with 40 contours and 8000 nodes per contour.

6. Summary and conclusion

We have newly implemented contour dynamics method for the Vlasov-Poisson system with the periodic boundary. The major difficulty in application of the periodic boundary is how to deal with contours when they cross the boundaries. It has been overcome by introducing periodic Green's function defined on the infinite phase space, instead of the Green's function derived for the bounded system with the periodic boundary condition. The new scheme enables implementation without cutting nor reallocating the contours and node points, and accelerates the computational speed.

Validity of the CD method for the Vlasov-Poisson system with the periodic boundary is confirmed by comparing the simulation results with the analytical solution for the piece-wise constant distribution function in the linear regime, and by the bench mark test for the linear Landau damping. Nonlinear Landau damping simulation using the CD method successfully reproduces the electron trapping by the Langmuir wave. Soundness of our method is also demonstrated by the energy and particle conservation with errors less than 2.5×10^{-5} and 10^{-4}, respectively, when one used 40 contours with 8000 nodes per contour. Improvement of the CD method to reduce the conservation errors remains for future works.

Because this paper focused on the verification of our basic CD scheme for the periodic system, detailed analyses of the physics problem by means of the CD method are remained for future studies. Application of the CD method to a variety of issues in kinetic plasma physics is currently in progress, and will be reported elsewhere.

CRediT authorship contribution statement

Hiroki Sato: Formal analysis, Investigation, Methodology, Software, Writing – original draft. **T.-H. Watanabe:** Conceptualization, Funding acquisition, Methodology, Supervision, Writing – review & editing. **S. Maeyama:** Conceptualization, Supervision, Writing – review & editing.

Declaration of competing interest

The authors declare that they have no known competing financial interests or personal relationships that could have appeared to influence the work reported in this paper.

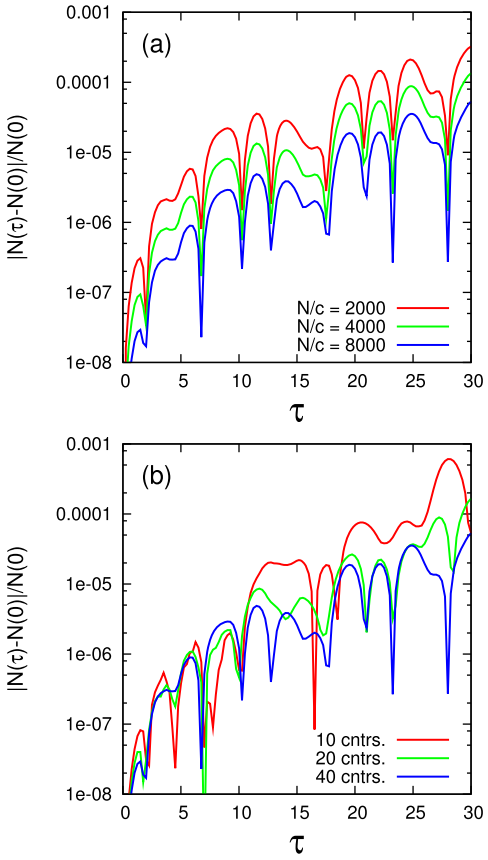

Fig. 9. Errors found in the particle conservation, $|N(\tau) - N(0)|/N(0)$, for cases with different numbers of (a) nodes per a contour (that is, 2000, 4000, and 8000 with 40 contours) or (b) contours (that is, $N_{Max} = 10$, 20, and 40 with 8000 nodes per contour but $dv = 0.4$, 0.2, and 0.1, respectively). Blue curves in (a) and (b) represent the same result in the case with 40 contours and 8000 nodes per a contour.

Acknowledgements

This work is supported by JSPS KAKENHI Grant Number JP16H04086. A part of numerical computations is performed using the computer resource of Plasma Simulator of National Institute for Fusion Science (NIFS) with the support and under the auspices of the NIFS Collaboration Research program (NIFS20KNST178).

Appendix A

Here, we calculate the analytical solution of $a(x, \tau) = \partial\phi/\partial x$ for the initial distribution function in Eqs. (29) and (30). For a node with the index m, v_m satisfies the equation

$$a(x, \tau) = \frac{dv_m}{d\tau} = \frac{\partial v_m}{\partial \tau} + v_m \frac{\partial v_m}{\partial x}. \tag{40}$$

Eqs. (8) and (29) lead to

$$-\frac{\partial a}{\partial x} = 1 - \sum_{-N_m}^{N_m} (-b_m)\, v_m. \tag{41}$$

For the zeroth order, the electron density is assumed to be the same as that of the uniform background ions, $\sum_{-N_m}^{N_m} (-b_m)\, v_m^0 = 1$ (namely, we choose Δv to satisfy this relation). Therefore, Eq. (40) is linearized as

$$a = \frac{\partial v_m^1}{\partial \tau} + v_m^0 \frac{\partial v_m^1}{\partial x}, \tag{42}$$

and Eq. (41) reads

$$\frac{\partial a}{\partial x} = \sum_{-N_m}^{N_m} (-b_m)\, v_m^1. \tag{43}$$

Assuming $a, v_m^1 \propto e^{ikx}$, the Laplace transform of Eqs. (42) and (43) give

$$L(a) = -v_m^1(0) + sL\left(v_m^1\right) + v_m^0 ikL\left(v_m^1\right), \tag{44}$$

$$-ikL(a) = \sum_{-N_m}^{N_m} b_m L\left(v_m^1\right), \tag{45}$$

where $L\left(f\left(\tau\right)\right) := \int_0^\infty f(\tau) e^{-s\tau} d\tau$. Thus,

$$L(a) = \frac{1}{D(is)} \sum_{-N_m}^{N_m} \left\{ (-b_m)\, v_m^1(0) \Pi_{l\neq m} \left(is - kv_l^0 \right) \right\}, \tag{46}$$

with

$$D(is) = k\Pi_{m=-N_m}^{N_m} \left(is - kv_m^0 \right) + \sum_{m=-N_m}^{N_m} \left\{ b_m \Pi_{l\neq m} \left(is - kv_l^0 \right) \right\}. \tag{47}$$

It is known that for a choice of $b_n < 0$ ($\forall n \geq 1$), the solutions of $D(is) = 0$ are purely real (see Refs. [11] and [12]). We define $\omega := is$ and $\omega_m : D(\omega_m) = 0$ with $kv_m^0 < \omega_m < kv_{m+1}^0$ so that $D(\omega_m)$ is written as $D = k\Pi_{m=-N_m}^{N_m}(\omega - \omega_m)$. The inverse Laplace transform of Eq. (46) is

$$a = \sum_{j=-N_m}^{N_m} Res\left(L\left(a\right)(s)\, e^{st}, -i\omega_j \right) \tag{48}$$

$$= \sum_{j=-N_m}^{N_m} \lim_{s\to -i\omega_j} \left(s + i\omega_j\right) \frac{1}{k} \frac{\sum_{-N_m}^{N_m} \left\{ (-b_m)\, v_m^1(0) \Pi_{l\neq m} \left(is - kv_l^0 \right) \right\}}{\Pi_{m=-N_m}^{N_m} \left(is - \omega_m\right)} e^{st} \tag{49}$$

Since $\omega_m = -\omega_{-m}, b_m = -b_{-m}$ and $v_m^0 = -v_{-m}^0$, one finds

$$a(x,\tau) = Re\left[\sum_{j>0} \frac{\sum_{m>0} \left\{ (-b_m)\, \alpha e^{i(kx - \frac{\pi}{2})} \Pi_{n(\neq m)>0} \left(\left(\omega_j\right)^2 - \left(kv_n^0\right)^2 \right) \right\}}{k\Pi_{n(\neq j)>0} \left(\omega_j^2 - \omega_n^2 \right)} 2\cos\omega_j\tau \right], \tag{50}$$

where ω_j satisfies the dispersion relation of

$$1 + \sum_{m>0} \frac{2b_m v_m^0}{\omega^2 - \left(kv_m^0\right)^2} = 0. \tag{51}$$

References

[1] T-H. Watanabe, Hideo Sugama, Vlasov and drift kinetic simulation methods based on the symplectic integrator, Transp. Theory Stat. Phys. 34 (3–5) (2005) 287–309.
[2] K.V. Roberts, H.L. Berk, Nonlinear evolution of a two-stream instability, Phys. Rev. Lett. 19 (Aug 1967) 297–300.
[3] D.C. DePackh, The water-bag model of a sheet electron beamy, Int. J. Electron. 13 (5) (1962) 417–424.
[4] Pierre Morel, Etienne Gravier, Nicolas Besse, Alain Ghizzo, Pierre Bertrand, The water bag model and gyrokinetic applications, Commun. Nonlinear Sci. Numer. Simul. 13 (1) (2008) 11–17.
[5] Norman J. Zabusky, M.H. Hughes, K.V. Roberts, Contour dynamics for the Euler equations in two dimensions, J. Comput. Phys. 30 (1) (1979) 96–106.
[6] Stefan G. Llewellyn Smith, Ching Chang, Tianyi Chu, Mark Blyth, Yuji Hattori, Hayder Salman, Generalized contour dynamics: a review, Regul. Chaotic Dyn. 23 (5) (2018) 507–518.
[7] Stéphane Colombi, Jihad Touma, Vlasov–Poisson: the waterbag method revisited, Commun. Nonlinear Sci. Numer. Simul. 13 (1) (2008) 46–52.
[8] David G. Dritschel, Contour surgery: a topological reconnection scheme for extended integrations using contour dynamics, J. Comput. Phys. 77 (1) (1988) 240–266.
[9] Pauline Wilhelmina Catharina Vosbeek, Robert Martinus Maria Mattheij, Contour dynamics with symplectic time integration, J. Comput. Phys. 133 (2) (1997) 222–234.
[10] Ivar Stakgold, Michael J. Holst, Green's Functions and Boundary Value Problems, vol. 99, John Wiley & Sons, 2011.
[11] G. Rowlands, Landau damping and the water-bag model, Phys. Lett. A 30 (7) (1969) 408–409.
[12] D.E. Baldwin, G. Rowlands, Plasma oscillations perpendicular to a weak magnetic field, Phys. Fluids 9 (12) (1966) 2444–2453.